NASA

ALUMINUM CHLORINE BATTERY

BY JOSÉ GINER AND GERHARD L. HOLLECK

DECEMBER 1969

Prepared under Contract No. NAS 12-688 by

TYCO LABORATORIES, INC.
WALTHAM, MASSACHUSETTS 02154

ELECTRONICS RESEARCH CENTER
NATIONAL AERONAUTICS AND SPACE ADMINISTRATION

Dr. Sol Gilman, CPE
Technical Monitor
NASA, Energy Conversion Branch
Electronics Research Center
575 Technology Square
Cambridge, Massachusetts 02139

Requests for copies of this report should be referred to:

NASA Scientific and Technical Information Facility
P. O. Box 33
College Park, Maryland 20740

NASA

ALUMINUM CHLORINE BATTERY

By José Giner and Gerhard L. Holleck

Sixth Quarterly Report
Covering Period
27 August 1969 — 26 December 1969

Prepared under Contract No. NAS 12-688 by

TYCO LABORATORIES, INC.
WALTHAM, MASSACHUSETTS 02154

Electronics Research Center
NATIONAL AERONAUTICS AND SPACE ADMINISTRATION

Table of Contents

Section	Page No.
SUMMARY	1
INTRODUCTION	1
PURIFICATION OF $AlCl_3$-KCl-NaCl MELTS	3
CONDUCTIVITY MEASUREMENTS IN $AlCl_3$-KCl-NaCl	4
Experimental	4
Results	4
EFFECT OF MASS TRANSPORT AT THE Al ELECTRODE	9
The Rotating Disk Arrangement	9
Results	9
RELATION BETWEEN CURRENT AND ACTIVATION POLARIZATION	13
Galvanostatic Current Step Methods	13
Experimental	15
Results	15
REFERENCES	24

List of Illustrations

Figure No.		Page No.
1.	Pyrex Capillary Conductivity Cell	5
2.	Specific Conductivity of $AlCl_3$-KCl-NaCl (57.5-12.5-30 Mol %) as a Function of Temperature	6
3.	Rotating Disk Electrode Arrangement	10
4.	Schematic Diagram of Rotating Disk Electrode	10
5.	Anodic Limiting Current at Rotating Al Disk as a Function of Rotation Rate	12
6.	Schematic Diagram of Measuring Circuit for Galvanostatic Pulse Experiments	16
7.	Anodic, Galvanostatic, Potential-Time Curve on Al Electrode in $AlCl_3$-KCl-NaCl (57.5-12.5-30 Mol %) at 130 °C	17
8.	Cathodic, Galvanostatic, Potential-Time Curve on Al Electrode in $AlCl_3$-KCl-NaCl (57.5-12.5-30 Mol %) at 130 °C	17
9.	Variation of Overvoltage With Time at the Al Electrode Upon a Galvanostatic Current Step in $AlCl_3$-KCl-NaCl (57.5-12.5-30 Mol %) at 130 °C (Dashed Lines = $t_c^{1/2}$)	18
10.	Current Density Versus Activation Overvoltage at Al Electrode in $AlCl_3$-KCl-NaCl (57.5-12.5-30 Mol %) at 130 °C	21
11.	Allen-Hickling Plot of Current-Potential Data at Al Electrode in $AlCl_3$-KCl-NaCl (57.5-12.5-30 Mol %) at 130 °C	22

List of Illustrations (Cont.)

Figure No.		Page No.
11.	Differential Thermal Analysis Curves (Al_2O_3 Reference; Heating Rate = 4°/min)	16
12.	Cut Through $AlCl_3$-Rate Part of $AlCl_3$-KCl-NaCl Phase Diagram (Preliminary Measurements)	17

ALUMINUM CHLORINE BATTERY

By José Giner and Gerhard L. Holleck

Tyco Laboratories, Inc.
Waltham, Massachusetts 02154

SUMMARY

The purification procedure for $AlCl_3$, described in our earlier reports, was modified by producing finely divided Al in situ in order to reduce the ionic iron content of the melt before evaporation of the $AlCl_3$.

Measurements of electrolyte conductivity were made in the ternary melt. The temperature dependence of the specific conductivity from 125 to 185 °C in the $AlCl_3$-KCl-NaCl melt (57.5-12.5-30 mol %) can be represented by

$$\kappa_{sp} = 11.4 \pm 0.9 \exp\left(-\frac{3360 \pm 68}{RT}\right) \text{ohm}^{-1}\text{cm}^{-1}$$

The currents at the Al electrode were limited almost solely by mass transport, as was shown by studies at a rotating disk electrode. The electrode processes were further investigated by galvanostatic, current step methods. It was found that the charge transfer step at the Al electrode was quite fast, and that the observed overvoltages were mainly due to concentration polarization. The apparent exchange current, i_0, at 130 °C was determined to be 268 mA/cm^2, and the average double layer capacity was found to be 40 $\mu F/cm^2$.

INTRODUCTION

The aim of the present contract is to show both the potential and the problems inherent in a molten salt system based on an Al anode and Cl_2 cathode in an $AlCl_3$-alkali chloride melt (which we have prepared). This system offers promise as a rechargeable, high energy density battery.

To obtain pure $AlCl_3$-KCl-NaCl melts, different commercial aluminum chloride materials have been investigated. $FeCl_3$ was found to be the major impurity in all of them. A procedure involving treatment of a melt of high $AlCl_3$ concentration

with magnesium powder prior to evaporation yielded pure $AlCl_3$. $AlCl_3$-KCl-NaCl melts using this material stayed clear (nearly colorless), and showed practically no background current.

Investigations of vitreous carbon electrodes have shown that carbon is intrinsically active for chlorine reduction in $AlCl_3$-alkali chloride melts. A study of the compatibility of carbon electrodes with chlorine in $AlCl_3$ eutectics has uncovered carbon samples which appear suitable for the construction of porous chlorine cathodes.

More recently, our attention was directed towards the processes occurring at the Al electrode in $AlCl_3$-KCl-NaCl melts. Passivation phenomena have been observed upon cathodic and anodic polarization. It was established that they were not due to an electrochemical (potential-dependent) process, but rather were caused by formation of a solid salt layer at the electrode surface resulting from concentration changes upon anodic or cathodic current flow. The value of the steady-state current was determined by diffusion processes in the melt and the concentration change necessary to pass the liquidus curve of the phase diagram. The electrode behavior upon cathodic polarization was further complicated by dendrite growth, which caused the electrode to expand into the melt.

In the present reporting period, we continued to investigate the kinetic behavior of the Al electrode, the effect of mass transport, and the conductivity of the melt.

PURIFICATION OF $AlCl_3$-KCl-NaCl MELTS

The purification procedure for $AlCl_3$, described in our earlier report, was modified by producing finely divided Al in situ in order to reduce the ionic iron content of the melt before evaporation of the $AlCl_3$. A quartz rack containing three electrodes (an Al wire in the center, an Al sheet cylinder as counterelectrode, and a Pt wire electrode) and a baffle were introduced into a 2-l kettle which was surrounded by a heating mantle and which contained a Teflon-coated, magnetic stirring bar. A 1500-g salt mixture of $AlCl_3$-KCl-NaCl (67.5-13.38-19.12 wt %) was introduced into the vessel. Between 130 and 140 °C, the resulting melt had only a moderate $AlCl_3$ vapor pressure.

By using a high current (~10 A) between the Al electrodes, dendrites were formed at the wire electrode and partially separated from the electrode upon current reversal. Thus, high surface Al was produced in situ. The melt was kept under constant stirring at 140 °C for 24 to 36 hr.

The progress of the exchange of Fe^{3+} for Al^{3+} was monitored by cyclic potential sweeps at the Pt wire electrode. A reduction in the ionic iron of more than a factor of 25 was obtained. This procedure was then followed by raising the temperature and evaporating the $AlCl_3$ into an aircooled, 1-l reaction kettle placed upside down on top of the reaction vessel, as described earlier.

CONDUCTIVITY MEASUREMENTS IN $AlCl_3$-KCl-NaCl

Experimental

For these measurements, we designed a capillary conductivity cell (shown schematically in Fig. 1) of Pyrex glass with platinized platinum electrodes. This was mounted in a test-tube-like vessel containing a side arm for the connection to the pressure-controlled Ar atmosphere. To ensure a uniform melt composition in the measuring capillary and in the remaining part of the vessel, the melt was mixed by forcing it out of the measuring section by a short application of positive Ar pressure to the center tube of the cell before each measurement. Temperature was measured by a thermocouple directly at the capillary (see Fig. 1). The whole arrangement was heated by a stirred silicone oil bath controlled to ±0.2 °C by a Matheson Lab Stat in conjunction with a two-stage heater. The assembling of the cell and handling of the melt were performed in the Ar atmosphere of the dry box. The cell resistance was measured by a precision ac bridge.

Results

The specific conductivity, κ_{sp}, is given by

$$\kappa_{sp} = \frac{a}{R} \ (\text{ohm}^{-1}\ \text{cm}^{-1})$$

where a is the cell constant and R is the measured resistance. The cell constant was determined in the standard way by using 1N KCl solution and the tabulated values for its conductivity (it was found to be 119.24 cm^{-1}). Generally, we used a measuring frequency of 1 kHz after establishing that the measured resistance values were independent of the ac frequency used (100 Hz to 10 kHz).

Table I shows the measured resistances and the specific conductivities of the $AlCl_3$-KCl-NaCl melt (57.5-12.5-30.0 mol %) which was used in many of our electrochemical investigations. Fig. 2 shows the temperature dependence of the conductivity data in an Arrhenius plot. These data can be represented very well by a straight line. A least-squares fit leads to:

$$\kappa_{sp} = 11.4 \pm 0.9 \exp\left(-\frac{3360 \pm 68}{RT}\right) \qquad (125 \text{ to } 185\ ^\circ\text{C})$$

where the given range represents the 95% confidence limits.

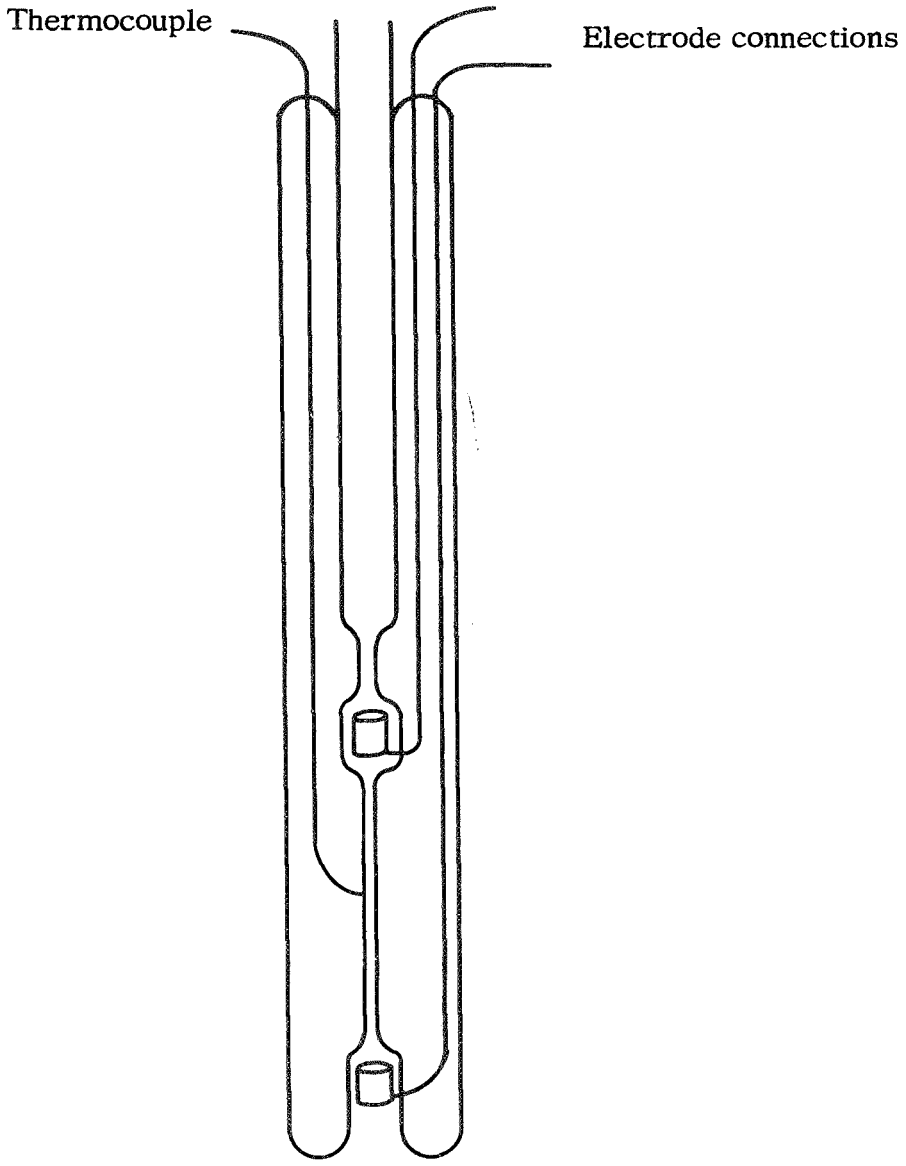

Fig. 1. Pyrex capillary conductivity cell

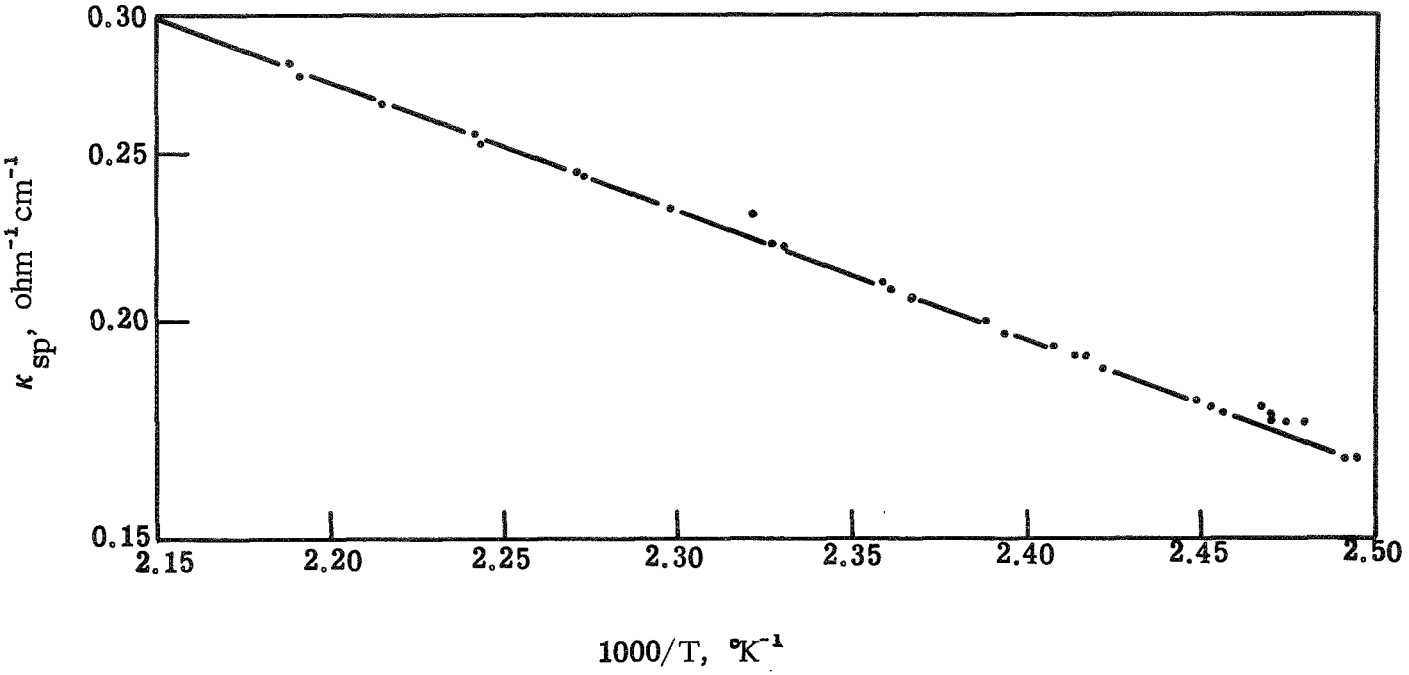

Fig. 2. Specific conductivity of $AlCl_3$-KCl-NaCl (57.5-12.5-30 mol %) as a function of temperature

TABLE I

SPECIFIC CONDUCTIVITY OF $AlCl_3$-KCl-NaCl (57.5-12.5-30.0 mol %)

Temperature, °C	Resistance, ohms	κ_{sp}, $ohm^{-1}cm^{-1}$
131.7	678	0.1758
131.7	681	0.1751
128.2	715	0.1667
127.8	715	0.1667
133.9	675	0.1766
133.9	672	0.1774
134.6	668	0.1785
135.0	662	0.1801
139.9	633	0.1883
140.6	625	0.1907
141.0	625	0.1907
144.6	605	0.1970
145.3	594	0.2007
149.4	577	0.2066
150.4	569	0.2095
150.4	568	0.2099
150.6	565	0.2110
156.0	541	0.2204
156.5	537	0.2220
157.4	515	0.2315
161.8	511	0.2333
166.8	490	0.2433
167.0	488	0.2443
172.5	468	0.2547
172.7	466	0.2558
178.3	446	0.2673
178.9	444	0.2685
183.2	432	0.2760
183.5	428	0.2786
142.2	641	0.1860
132.2	669	0.1782
131.2	680	0.1753
130.1	681	0.1751

Attempts are frequently made to relate the apparent activation energy obtained in this way to energy and entropy changes of postulated unimolecular rate processes. However, such a treatment would neglect changes in the density, and thus the spacings, of the salt with temperature. Nevertheless, the equation represents a very good interpolation formula within the temperature range of our data.

EFFECT OF MASS TRANSPORT AT THE Al ELECTRODE

The Rotating Disk Arrangement

An overall view of the rotating disk electrode setup is shown in Fig. 3. It consisted of a sturdy stand on which a 1/15-hp Bodine motor and a precision ball bearing for the 0.025-in. rotating shaft were mounted. The motor speed was controlled by a Minarik speed control (SL-52). The coupling of the motor and the electrode shaft was accomplished by a non-slip belt. The rotation rate of the electrode was continuously monitored by frequency modulation resulting from magnetic coupling of an electromagnet with an iron gear mounted on the rotating shaft. This signal was amplified and displayed on a frequency counter (Hewlett Packard model no. 5221A). Electrical contact to the disk electrode was accomplished through a mercury pool in the top of the rotating shaft.

The electrochemical cell was made of a 50-mm O-ring joint with a 30-mm-thick Teflon cover. The Teflon cover contained tapered holes to accommodate a liquid seal in the center with a 29/40 standard tapered joint surrounded by four 10/30 joints for gas inlet and outlet as well as the counter- and reference electrodes. A Teflon bell was fixed to the rotating shaft (Fig. 4). Mercury and silicone oil with a very low vapor pressure were used as sealant liquids.

The rotating electrode consisted of a cylindrical piece of pure Al press-fitted into hot Teflon. Details of the electrode construction are shown in Fig. 4. A sheet of pure Al of approximately 15 cm^2 was used as the counterelectrode, and an Al wire served as the reference electrode.

The electrochemical cell was held at a constant temperature by a stirred silicone oil bath. Temperature was controlled to ±0.2 °C by a Matheson Lab Stat proportional temperature control unit and a two-stage heating arrangement. As in all earlier measurements, the cell was assembled in the dry box. During the experiments, an Ar atmosphere at a slightly positive pressure was maintained above the melt.

Results

All results of our stationary polarization measurements at Al electrodes indicate that the anodic limiting currents are a function of the mass transport in the melt. We therefore expected the anodic limiting currents to depend on the diffusion

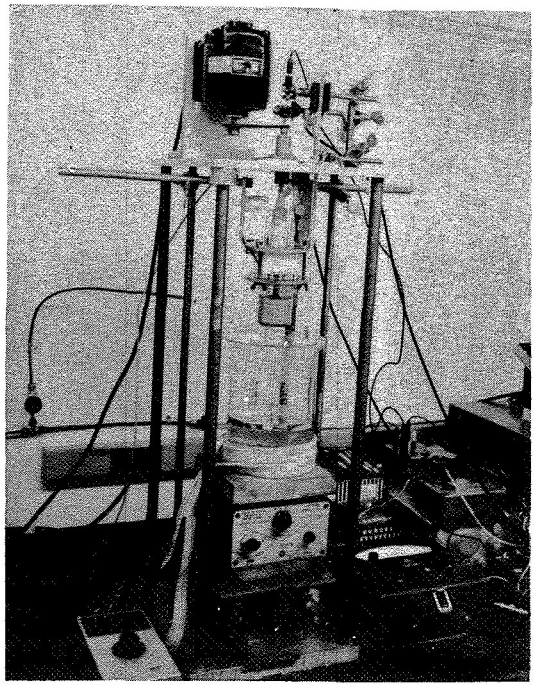

Fig. 3. Rotating disk electrode arrangement

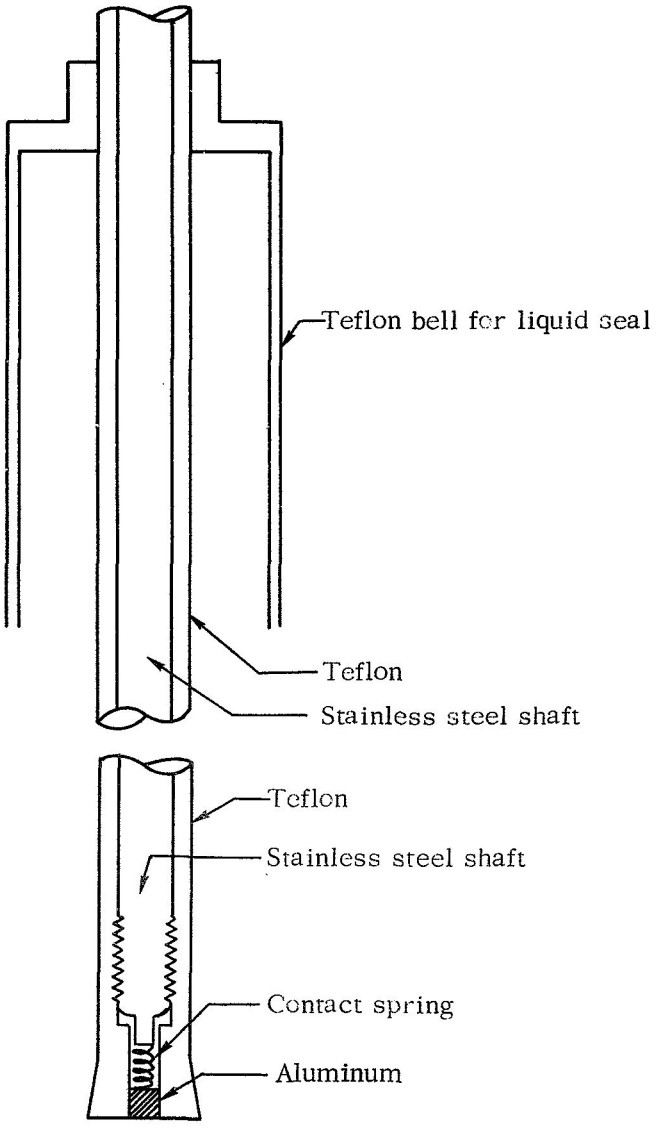

Fig. 4. Schematic diagram of rotating disk electrode

layer thickness and thus on the rotation rate of the rotating Al disk electrode.

The results of our experiments in $AlCl_3$-KCl-NaCl (57.5-12.5-30.0 mol %) at 125 °C are summarized in Fig. 5. This figure shows the variation of the anodic limiting current on the limiting plateau for different Al samples and different potentials as a function of the square root of the angular velocity.

The limiting current at a rotating disk electrode for a reaction controlled only by mass transfer is given by Levich (Ref. 1) as:

$$i_L = (\text{constant})\ nFD^{2/3}\ \upsilon^{-1/6}\ \omega^{1/2}\ \Delta c \qquad (1)$$

where the value of the constant is approximately 0.620, D is the diffusion coefficient, Δc is the concentration gradient of the electroactive species, υ is the viscosity, and $\omega = 2\pi$(rps), where rps = rotations per second. This equation implies a linear relationship between i_L and $\omega^{1/2}$ under diffusion controlled conditions.

As Fig. 5 shows, the experimental data can indeed be represented very well by a straight line. The slight deviations from linearity and some variation in the individual current densities were expected. One must keep in mind that here we are actually dealing with the dissolution of a passivating solid salt layer at the surface of the rotating electrode, which is in many respects quite different from the idealized conditions for which the above equation is strictly valid. Further, at the high current densities observed, changes in the electrode itself cannot be avoided. These results show clearly, however, the role of transport phenomena in removing reaction products from the electrode surface. They show further that high current densities can be obtained at Al electrodes at relatively low temperature if the transport limitations can be overcome.

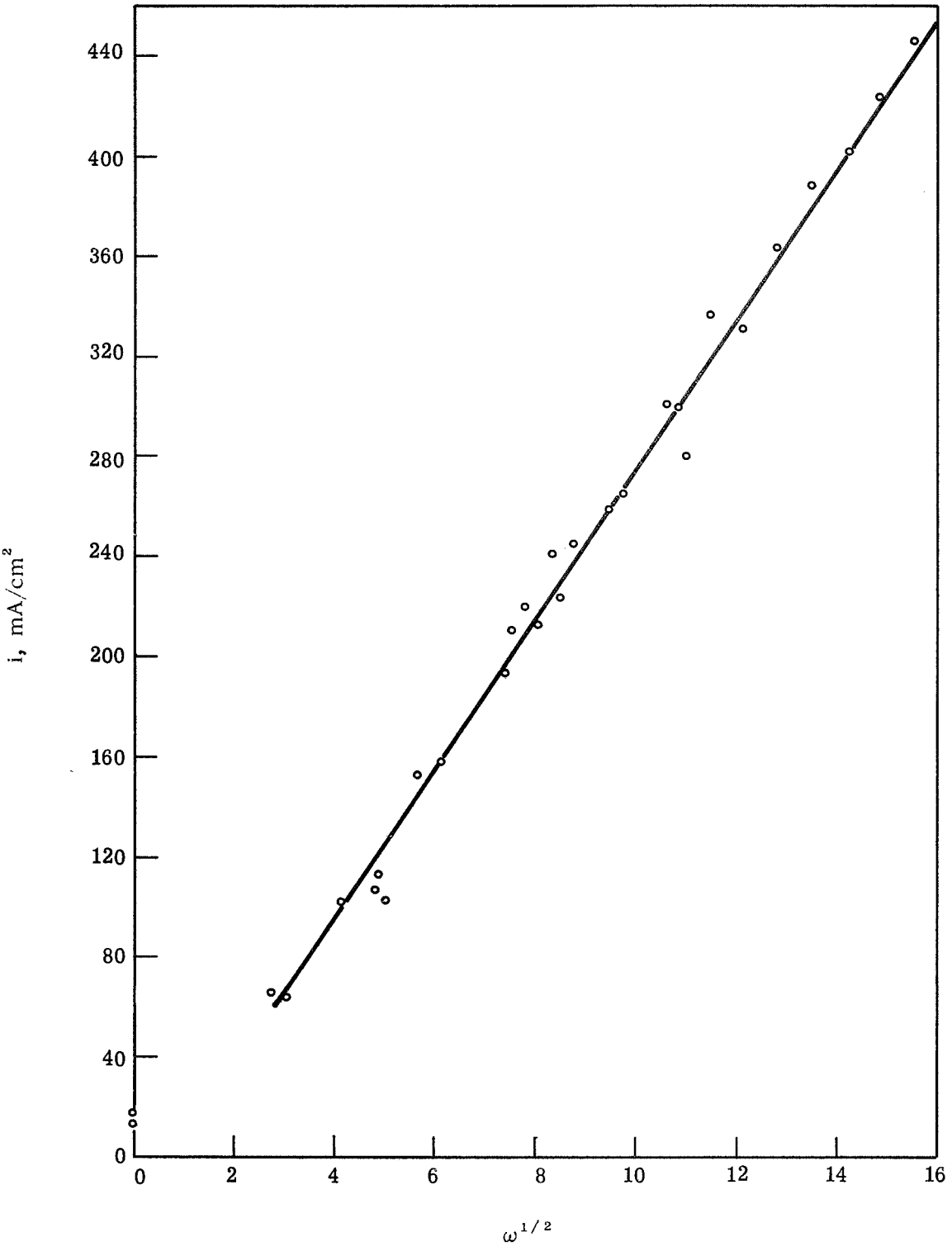

Fig. 5. Anodic limiting current at rotating Al disk electrode in $AlCl_3$-KCl-NaCl (57.5-12.5-30 mol %) at 125 °C as a function of rotation rate

RELATION BETWEEN CURRENT AND ACTIVATION POLARIZATION

Preliminary measurements showed that the charge transfer process at the Al electrode is quite fast. This means that the electrode process is very reversible and the observed overvoltages are mainly due to concentration polarization. It is therefore necessary to use transient methods to investigate the electrode kinetics. We chose galvanostatic pulse measurements for this purpose.

Galvanostatic Current Step Methods

The galvanostatic technique, considering the double layer charging, was originally discussed by Berzins and Delahay (Ref. 2). Since then, it has been used in several investigations (Ref. 3). The change in potential resulting from the constant current through the electrode-melt interface is determined by the rate of charging of the double layer and the rate of mass transfer to the electrode, i.e.:

$$i = C_{dl}\frac{d\eta}{dt} + nFD\left(\frac{\partial C_0}{\partial x}\right)_{x=0} \qquad (2)$$

where the symbols have their usual meaning. For a metal activity of unity and for the boundary conditions, $C_0 = C_0^\circ$ when $x > 0$ and $t = 0$, and $C_0 \rightarrow C_0^\circ$ when $x = \infty$ and $t \geq 0$:

$$nFD\left(\frac{\partial C_0}{\partial x}\right)_{x=0} = i_0\left\{\frac{C_0}{C_0^\circ}\exp\left(\frac{-\alpha n\eta F}{RT}\right) - \exp\left[\frac{(1-\alpha)n\eta F}{RT}\right]\right\} \qquad (3)$$

which gives

$$\eta = \frac{-i}{C_{dl}}\frac{1}{(A-B)}\left\{\frac{B}{A^2}\left[\exp(A^2t)\ \operatorname{erfc}(At^{1/2}) + \frac{2At^{1/2}}{\pi^{1/2}}\right]\right. \qquad (4)$$

$$\left. \times\frac{-A}{B^2}\left[\exp(B^2t)\ \operatorname{erfc}(Bt^{1/2}) + \frac{2Bt^{1/2}}{\pi^{1/2}} - 1\right]\right\}$$

for $\eta < (0.1\ RT/nF)$ ($\sim$5 mV), where

$$A = \frac{i_0}{2\ nFC_0^\circ D^{1/2}} + \left[\frac{i_0^2}{4\ n^2F^2\ (C_0^\circ)^2 D} - \frac{nFi_0}{RTC_{dl}}\right]^{1/2}$$

and

$$B = \frac{i_0}{2\,nFC_0^\circ D^{1/2}} - \left[\frac{i_0 2}{4\,n^2F^2(C_0^\circ)^2 D} - \frac{nFi_0}{RTC_{dl}}\right]^{1/2}$$

For $t > 50/B^2$, Eq. (4) approximates, within 1%, to

$$\eta = \frac{-2\,RTit^{1/2}}{\pi^{1/2}n^2F^2C_0^\circ D^{1/2}} + \frac{RTi}{nF}\left[\frac{RTC_{dl}}{n^3F^3(C_0^\circ)^2 D} - \frac{1}{i_0}\right] \qquad (5)$$

Hence, a plot of $\eta/t^{1/2}$ should give a straight line of slope

$$\frac{d\eta}{d(t^{1/2})} = \frac{-2\,RTi}{\pi^{1/2}n^2F^2C_0^\circ D^{1/2}} \qquad (6)$$

from which a value for $C_0^\circ D^{1/2}$ can be calculated.

When $t^{1/2} = 0$, then

$$\eta = \frac{RTi}{nF}\left[\frac{RTC_{dl}}{n^3F^3(C_0^\circ)^2 D} - \frac{1}{i_0}\right] \qquad (7)$$

and the intercept on the η axis, together with the value for $D(C_0^\circ)^2$ calculated above, will give a value for i_0 from Eq. (7).

An alternative method for calculating i_0 is the use of a special value of $t^{1/2}$ given by

$$t_c^{1/2} = -\frac{\pi C_{dl}}{4i} \times \frac{d\eta}{d\left(t^{1/2}\right)} \qquad (8)$$

The corresponding overpotential, η_c, can be found from the curve, and a value for i_0 calculated from the equation

$$\eta_c = -\frac{RT}{nF} \times \frac{i}{i_0} \qquad (9)$$

Both of these methods depend on the determination of the differential double layer capacity which can be ascertained by the initial slope of the voltage-time trace at sufficiently short times. One can show (Ref. 4) that for the error of C_{dl} to be less than m%, the maximum time, t_m, to which the measurement of the slope can be extended is $t_m = 2\,mRT\,C_{dl}/100\,nFi_0$. Thus, for example, if a double layer capaci-

tance of 40 μF is to be measured to better than 50% and i_0 = 250 mA/cm^2, then the slope of the potential-time trace has to be measured at times shorter than 2 μsec.

Experimental

In view of the facts mentioned above, it was necessary to use pulses with a very short rise time and high current density. It was also necessary to be able to record small potential changes with time, which required a low noise level in the experimental setup and the compensation of the ohmic potential drop in the solution. Fig. 6 shows a schematic of the measuring circuit. For the constant current pulses, the output of a Wavetek function generator was used directly. This instrument was gated by a Tyco-built pulse generator to allow multiple pulse application. By the use of two diodes, either cathodic or anodic current pulses could be selected. A dual trace oscilloscope (Tektronix 556 with two type W plug-in units) was used to record current and potential as a function of time. Current was measured by the potential drop across a known resistance. The i-R compensated potential-time traces were obtained by feeding the potential of the two-electrode cell and the output of the i-R compensator into the inputs of the differential amplifier. The measurements were conducted at an Al disk electrode (0.385 cm^2). A 15-cm^2 sheet of pure Al (Alpha Chemical Co.) served as the counterelectrode. The electrolyte was $AlCl_3$-KCl-NaCl (57.5-12.5-30.0 mol %). Since the freshly prepared melt showed some gassing, the temperature was raised and kept at 160 °C for about 2 hr. At that time, all gassing had stopped and the temperature of the melt was lowered to 130 °C and kept constant at this value by a temperature controlled silicone oil bath, as described earlier. Again, a slightly positive Ar pressure was kept in the cell at all times.

Results

Figs. 7 and 8 show two typical oscilloscopic potential-time traces at anodic and cathodic current pulses. From the initial slope of the galvanostatic voltage-time curves, we determined an average value for the double layer capacitance of 40 ± 10 μF/cm^2. Considering the surface roughness, one would expect to find a double layer capacitance of approximately this size in the absence of specific adsorption effects.

Fig. 9 is an example of overvoltage versus square root of time plots at various current densities, according to Eq. (5). At times larger than 10 μsec, the potential varies linearly with $t^{1/2}$. As expected, the slope of these lines increases

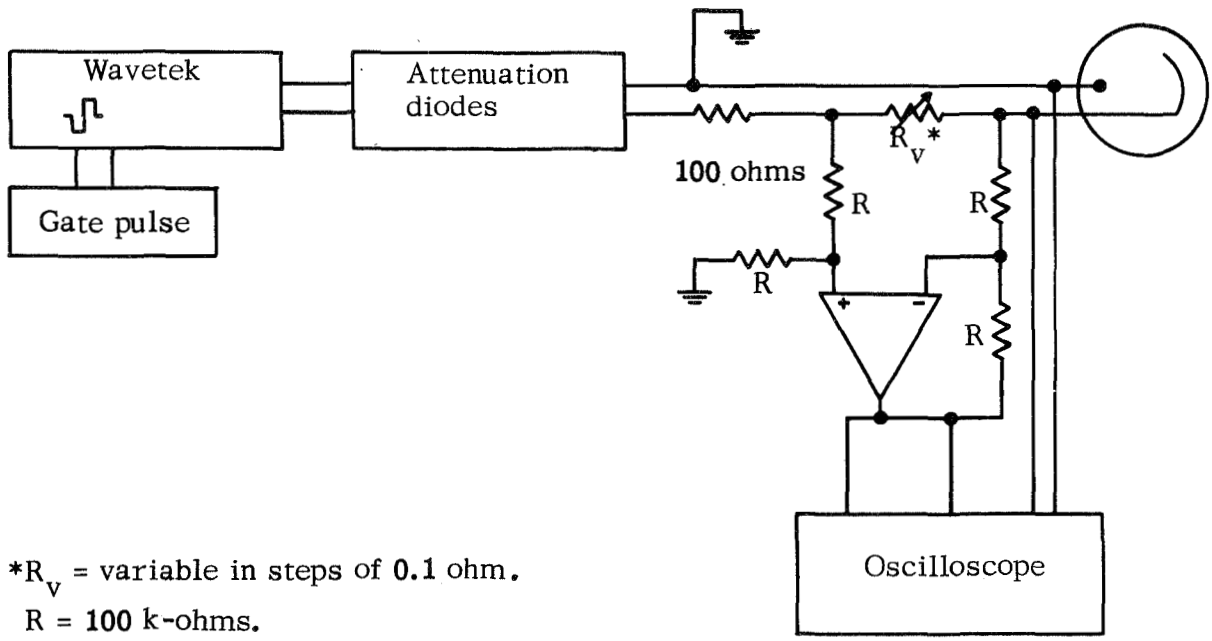

*R_V = variable in steps of 0.1 ohm.
R = 100 k-ohms.

Fig. 6. Schematic diagram of measuring circuit for galvanostatic pulse experiments

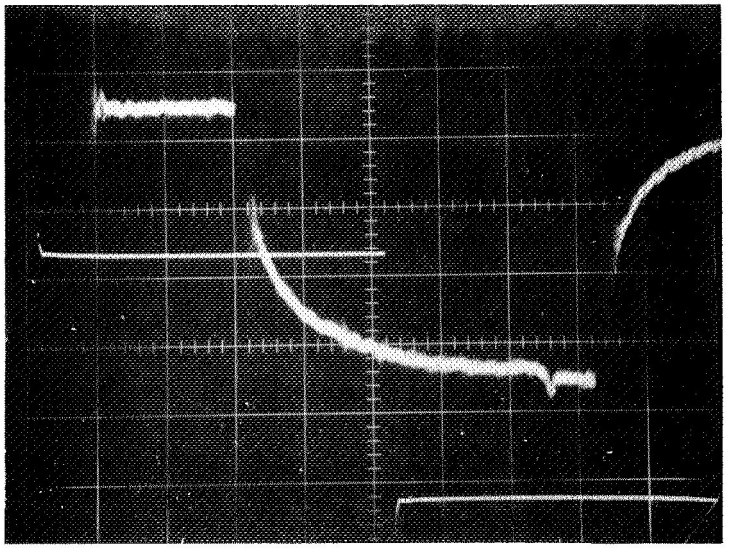

Fig. 7. Anodic, galvanostatic, potential-time curve on Al electrode in $AlCl_3$-KCl-NaCl (57.5-12.5-30 mol %) at 130 °C (i = 167 mA/cm^2, ordinate scale = 5 mV/div, abscissa scale = 10 μsec/div)

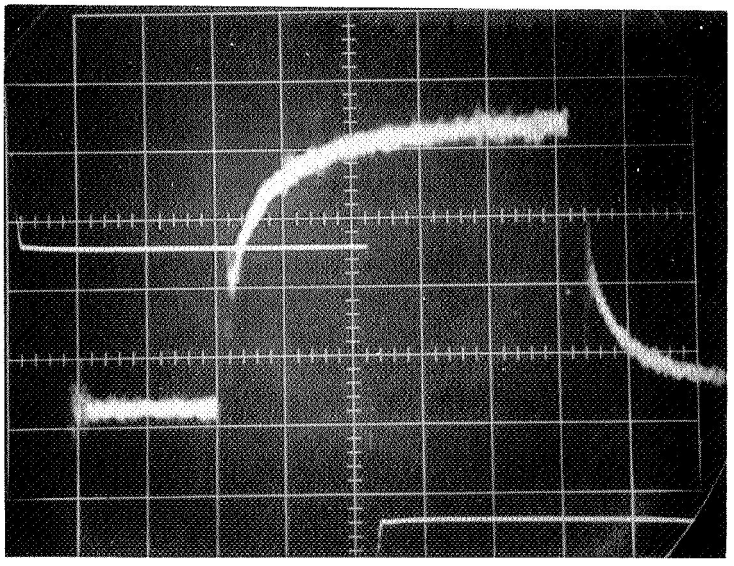

Fig. 8. Cathodic, galvanostatic, potential-time curve on Al electrode in $AlCl_3$-KCl-NaCl (57.5-12.5-30 mol %) at 130 °C (i = 185 mA/cm^2, ordinate scale = 5 mV/div, abscissa scale = 10 μsec/div)

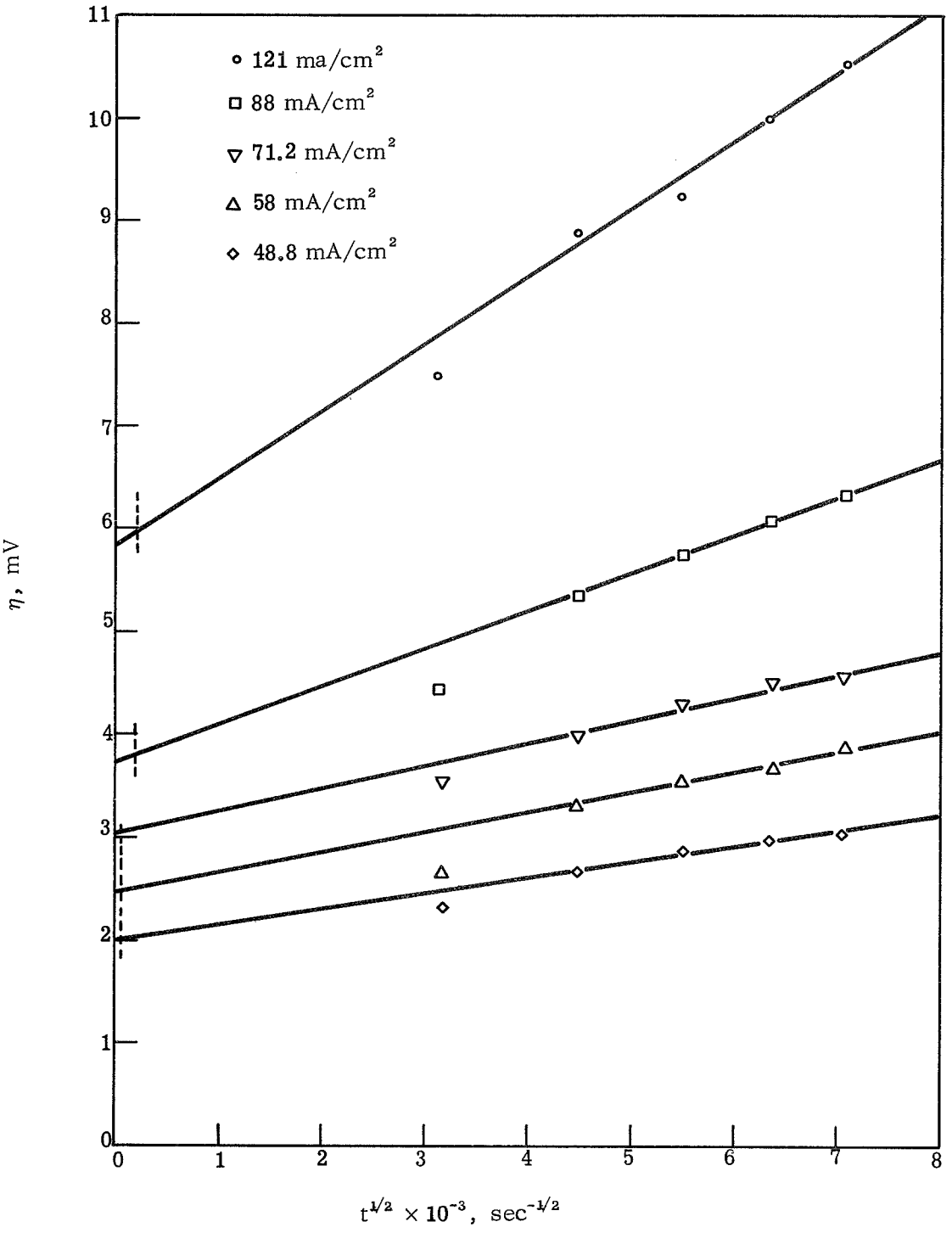

Fig. 9. Variation of overvoltage with time at the Al electrode upon a galvanostatic current step in $AlCl_3$-KCl-NaCl (57.5-12.5-30 mol %) at 130 °C (dashed lines = $t_c^{1/2}$)

with increasing current density. The times, $t_c^{1/2}$, according to Eq. (8) are also included in Fig. 9. The results of these measurements are summarized in Table II. The first column lists the current density (per geometric cm^2). The second column gives the overvoltages, η_c, obtained from a plot of η versus $t^{1/2}$ at time $t_c^{1/2}$. The third column gives values for the parameter $C_0^* D^{1/2}$ calculated from Eq. (6), using the slope of the straight lines from η versus $t^{1/2}$ plots. Finally, the last column gives values for the apparent exchange current calculated from Eq. (7). Fig. 10 shows a plot of i versus η.

At low overvoltage, one finds a linear relationship between current density and potential. From the slope at $\eta = 0$, one obtains again an exchange current according to Eq. (9). With $\eta = 3$, the apparent exchange current at the Al electrode was $i_0 = 268$ mA/cm^2 at 130 °C in the melt $AlCl_3$-KCl-NaCl (57.5-12.5-30.0 mol %). It is worth noting that there is no change in slope upon passing from anodic to cathodic overpotentials. This does not necessarily mean that we deal with the same rate determining step in the anodic and cathodic electrode reaction. It shows, however, that the anodic and cathodic exchange currents are equal.

If we assume that the cathodic and anodic rate determining steps are equal, the current-potential relationship can be represented by:

$$i = i_0 \{\exp(-\alpha z F \eta/RT) - \exp[(1-\alpha) z F \eta/RT]\} \qquad (10)$$

We can then use a plot which is valid regardless of the overvoltage, as was introduced by Allen and Hickling (Ref. 5). The above equation can be rewritten

$$\frac{i}{1-\exp(zF\eta/RT)} = i_0 \exp(-\alpha z F \eta/RT)$$

Thus

$$\ln \frac{i}{1-\exp(zF\eta/RT)} = \ln i_0 - \frac{\alpha z F}{RT}\eta \qquad (11)$$

The slope of a plot of Eq. (11) yields α, and the intercept at $\eta = 0$ gives the exchange current.

Fig. 11 shows a plot of Eq. (11), with the current-potential data obtained from the galvanostatic pulse measurements discussed above. The number of electrons transferred in the rate determining step, z, is varied from one to three. The calculated points can be represented fairly well by straight lines from whose slope one obtains the following values for α:

TABLE II

EXCHANGE CURRENTS AND MASS TRANSPORT FACTORS AT THE Al ELECTRODE

i, mA/cm^2	η_c, mV	i_0, mA/cm^2	$C_0^0 \times D^{1/2}$ $(mol/cm^2 sec^{1/2}) \times 10^{-8}$
		Anodic	
58	2.5	266	1.39
58		267	1.61
88	3.8	264	1.06
88		266	1.59
121	6.0	229	0.81
121		225	0.59
167	8.5	225	1.10
		Cathodic	
27.8	1.2	266	1.39
48.8	2.0	280	1.47
62.5	2.55	282	1.76
71.2	3.05	268	1.46
185.0	7.5	283	1.49
185.0	8.0	266	1.49

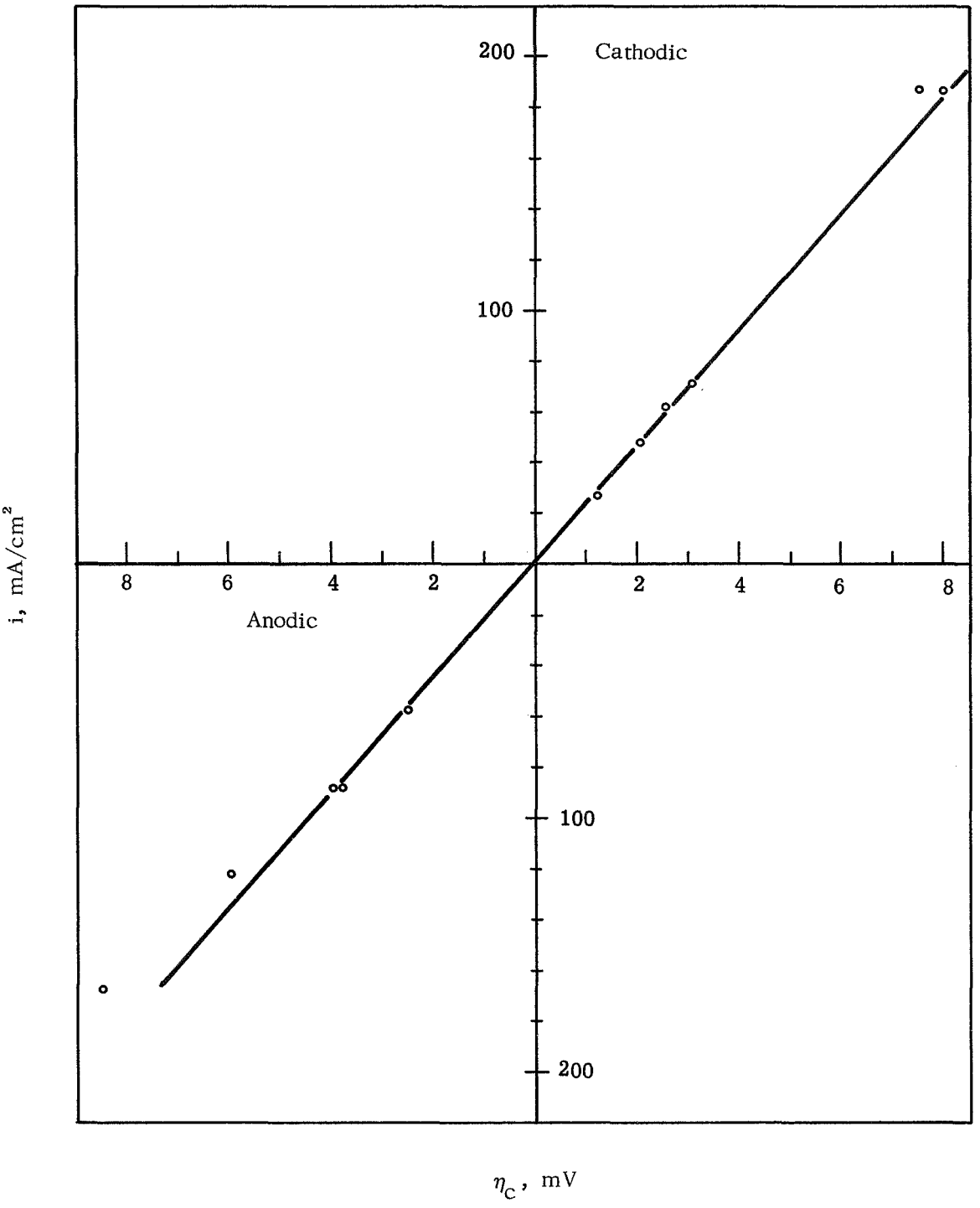

Fig. 10. Current density versus activation overvoltage at Al electrode in $AlCl_3$-KCl-NaCl (57.5-12.5-30 mol %) at 130 °C

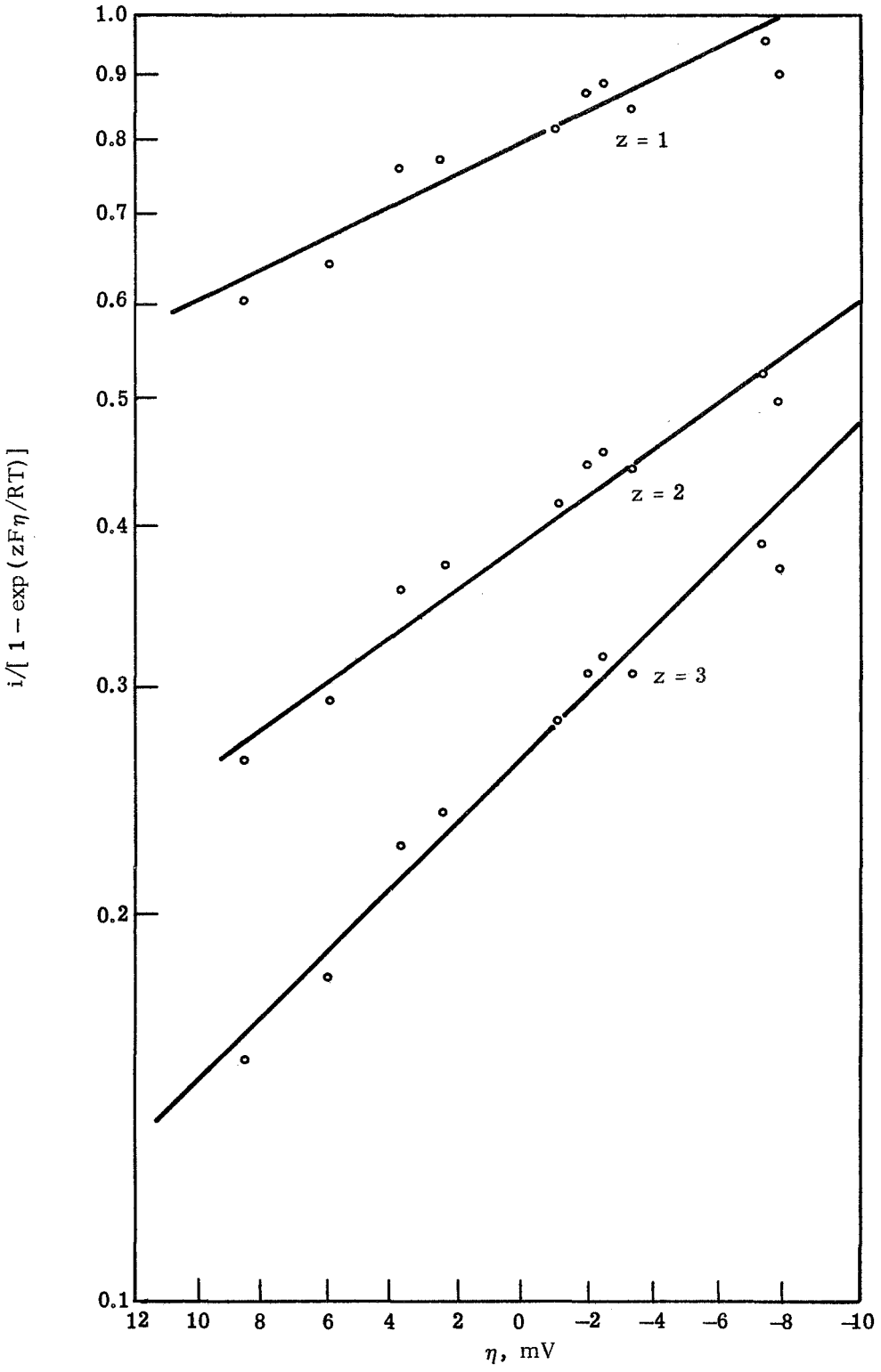

Fig. 11. Allen-Hickling plot of current-potential data at Al electrode in $AlCl_3$-KCl-NaCl (57.5-12.5-30 mol %) at 130 °C

z	α
1	1.0
2	0.7
3	0.64

Thus, the experimental results could be reasonably explained by a reversible two- or three-electron transfer step. Even though multiple electron transfer is less probable than the transfer of a single electron, it has been observed in molten salts (Ref. 6). The range of the presently available data is, however, not sufficient to decide upon a detailed mechanism of electron transfer at the Al electrode in the molten salt electrolyte.

Finally, it is quite interesting to examine more closely the values obtained for the transport parameter, $C_0^\circ D^{1/2}$. These values were found to be approximately 1.4×10^{-8}. Let us assume a diffusion coefficient of 10^{-6} cm^2/sec for the active species, similar to the value determined earlier for Fe^{3+}. Hence, one obtains $C_0 \approx 1.4 \times 10^{-5}$ mol/cm^3. For comparison, one can calculate the total $AlCl_3$ concentration in the melt to be $\sim 9.4 \times 10^{-3}$ mol/cm^3 (using an estimated value of 1.7 g/cm^3 for the density). Considering only the $AlCl_3$ not complexed as $KAlCl_4$ or $NaAlCl_4$, we would still have $\sim 1.2 \times 10^{-3}$ mol/cm^3 in our melt. Thus, the measured parameter $C_0^\circ D^{1/2}$ suggests a relatively low concentration of the electroactive species, probably caused by complex formation. Since practically nothing is known about complex formation in $AlCl_3$-rich melts, this interesting subject cannot be discussed further.

Recently, Del Duca investigated the electrochemical behavior of the Al electrode in molten $AlCl_3$-NaCl and $AlCl_3$-(LiCl-KCl) eutectic electrolytes in the temperature range 175 to 313 °C (Ref. 7). The apparent exchange currents varied from 1 to 56 mA/cm^2, and surface diffusion was found to be the rate determining step at low overpotentials. At high overpotentials, the most probable anodic rate determining step was given as $Al \rightarrow Al^+ + e^-$, and the most probable cathodic rate determining step in $AlCl_3$-NaCl electrolyte was given as $Al^{2+} + e^- \rightarrow Al^+$.

REFERENCES

1. Levich, V. G.: Physicochemical Hydrodynamics. Prentice Hall, Inc., 1962. For a review of the rotating disk system see Riddiford, A. C.: The Rotating Disk System, in Advances in Electrochemistry and Electrochemical Engineering, Vol. 4. P. Delahay, ed., Interscience, 1966.

2. Berzins, T., and Delahay, P.: J. Amer. Chem. Soc., 77, 6448 (1955); Z. Electrochem., 59, 792 (1955).

3. Graves, A. D., Hills, G. J., and Inman, D.: Electrode Processes in Molten Salts, in Advances in Electrochemistry and Electrochemical Engineering, Vol. 4. P. Delahay, ed., Interscience, 1966.

4. Inman, D., Bockris, J. O'M., and Blourgran, E.: J. Electroanal. Chem., 2, 506 (1961).

5. Allen, P. L., and Hickling, A.: Trans. Faraday Soc., 53, 1626 (1957).

6. Senderoff, S. and Mellors, G. W.: J. Electrochem. Soc., 113, 66 (1966).

7. Del Duca, B. S.: NASA TN D-5503, NASA, Washington, D. C., October 1969.